

Efficient computation of the second-Born self-energy using tensor-contraction operations

Riku Tuovinen*, Fabio Covito and Michael A. Sentef

Max Planck Institute for the Structure and Dynamics of Matter,
Luruper Chausse 149, 22761 Hamburg, Germany

Abstract. In the nonequilibrium Green's function approach, the approximation of the correlation self-energy at the second-Born level is of particular interest, since it allows for a maximal speed-up in computational scaling when used together with the Generalized Kadanoff-Baym Ansatz for the Green's function. The present day numerical time-propagation algorithms for the Green's function are able to tackle first principles simulations of atoms and molecules, but they are limited to relatively small systems due to unfavourable scaling of self-energy diagrams with respect to the basis size. We propose an efficient computation of the self-energy diagrams by using tensor-contraction operations to transform the internal summations into functions of external low-level linear algebra libraries. We discuss the achieved computational speed-up in transient electron dynamics in selected molecular systems.

PACS: 31.15.-p, 31.25.-v, 71.10.-w

Key words: Nonequilibrium Green's functions, second-Born self-energy, numerical algorithm

1 Introduction

A state-of-the-art computational method for out-of-equilibrium many-body physics is the nonequilibrium Greens function (NEGF) approach [1–5]. Mostly due to lack of computational capabilities, the non-linear integro-differential Kadanoff-Baym equations (KBE) for the NEGF from the 1960s remained fairly elusive until their first numerical implementations at the turn of the century [6–8]. During the past twenty years a considerable amount of progress has been achieved in various fields of physics employing the NEGF approach: From sub-atomic nuclear reactions [9, 10] to atomic and molecular scale [11–14], further to condensed phase [15–25] and mesoscopic systems [26–31], and even to descriptions of high-energy particle physics in cosmology [32–34].

However, combining the KBE with *ab initio* descriptions of realistic materials still remains a computational challenge. This challenge results from the double-time structure

*Corresponding author. *Email addresses:* riku.tuovinen@mpsd.mpg.de (R. Tuovinen), fabio.covito@mpsd.mpg.de (F. Covito), michael.sentef@mpsd.mpg.de (M. A. Sentef)

of the KBE rendering the method very expensive for both CPU time and storing the objects in RAM. The Generalized Kadanoff–Baym Ansatz (GKBA) offers a simplification by reducing the two-time-propagation of the Green’s function to the time-propagation of a time-local density matrix [35]. The computational complexity of the time-propagation of the GKBA equations scales as the number of time steps squared instead of the cubic scaling in the double-time KBE [36]. When a simulation to reach longer time scales is desired, this difference in computational speed becomes immense. However, this speed-up in computational scaling is only possible for the correlation self-energy approximation at the second-Born (2B) level. The 2B approximation goes beyond mean-field description at the Hartree-Fock (HF) level but it includes the bare interaction only up to second order, i.e., higher order correlations and screening effects are neglected, like in higher order T -matrix or GW approximations [37,38]. However, the viability of the 2B approximation has been assessed for a large set of systems with up to moderate interaction strength [39,40].

Even though the above implementations of the NEGF method have been successfully applied in many contexts, the computation of the self-energy still remains a numerical bottleneck. For larger systems to be studied, the scaling with respect to the basis size in the self-energy diagrams may be very unfavourable, making first principles simulations numerically expensive, at least in naïve implementations when looping over the full basis. Recently, a dissection algorithm has been proposed and implemented [41,42] for identifying and utilizing the sparsity of many-body interactions. In this paper we propose to transform the summation expressions in the self-energy diagrams using tensor-contraction operations, and to further employ external linear algebra libraries (e.g. low-level C or Fortran) taking into account, e.g., memory availability, communication costs, loop fusion and ordering [43–45]. (Here we consider *tensors* simply as multidimensional objects without deeper (differential-)geometric interpretation.) With benchmark simulations in selected molecular systems we present an efficient way to compute the 2B self-energy applicable either in full time-propagation of the KBE or in the numerically less expensive GKBA variant.

2 Model and method

We consider a finite and quantum-correlated electronic system described by a time-dependent Hamiltonian

$$\hat{H}(t) = \sum_{ij} h_{ij}(t) \hat{c}_i^\dagger \hat{c}_j + \frac{1}{2} \sum_{ijkl} v_{ijkl}(t) \hat{c}_i^\dagger \hat{c}_j^\dagger \hat{c}_k \hat{c}_l, \quad (2.1)$$

where i, j, k, l label a complete set of one-particle states $\{\varphi(\mathbf{r})\}$, and $\hat{c}^{(\dagger)}$ are the annihilation (creation) operators for electrons from (to) these states. Although we assume, for simplicity, spin-compensated electrons and invariance under spin rotations, the whole consideration could easily be generalized to include also spin degrees of freedom [39,46–48]. The

objects henceforth described will be diagonal in spin space. The one-body contribution to the Hamiltonian,

$$h_{ij}(t) = \int d\mathbf{r} \varphi_i^*(\mathbf{r}) h(\mathbf{r}, t) \varphi_j(\mathbf{r}), \quad (2.2)$$

may have an explicit time dependence, describing, e.g., pump-probe spectroscopies or voltage pulses. These would enter in $h(\mathbf{r}, t) = -\frac{1}{2}\nabla^2 + w(\mathbf{r}, t) - \mu$ as external fields w . We also introduced the chemical potential μ and we absorbed it into the equilibrium description of the one-body part of the Hamiltonian. Atomic units, $\hbar = m = e = 1$, are used throughout. The two-body part accounts for interactions between the electrons with the standard two-electron Coulomb integrals

$$v_{ijkl} = \int d\mathbf{r} \int d\mathbf{r}' \frac{\varphi_i^*(\mathbf{r}) \varphi_j^*(\mathbf{r}') \varphi_k(\mathbf{r}') \varphi_l(\mathbf{r})}{|\mathbf{r} - \mathbf{r}'|}. \quad (2.3)$$

Even though the Coulomb interaction itself is instantaneous, in Eq. (2.1) we allow the strength of the two-body part to be time-dependent to describe, e.g., interaction quenches or adiabatic switching. For real-valued basis functions φ the Coulomb integrals in Eq. (2.3) follow 8-point permutation symmetry

$$v_{ijkl} = v_{jilk} = v_{klij} = v_{lkji} = v_{ikjl} = v_{ljk i} = v_{kilj} = v_{jlik}, \quad (2.4)$$

which can be verified by permuting dummy integration variables and by complex conjugation. The following discussion is not limited to this choice, however, and also complex and spin-dependent basis functions could be used.

To calculate time-dependent nonequilibrium quantities we use the equations of motion for the one-particle Green's function on the Keldysh contour γ [3–5]. This object is defined as

$$G_{ij}(z, z') = -i \langle T_\gamma [\hat{c}_i(z) \hat{c}_j^\dagger(z')] \rangle, \quad (2.5)$$

where T_γ is the contour ordering operator and the variables z, z' specify the location of the Heisenberg-picture operators \hat{c} on the Keldysh contour. The contour has a forward and a backward branch on the real-time axis, $[t_0, \infty[$, and also a vertical branch on the imaginary axis, $[t_0, t_0 - i\beta]$ with inverse temperature β . The Green's function includes exhaustive information about particle propagation, and important physical quantities such as electric currents or photoemission spectra can be extracted from it. The Green's function G satisfies the integro-differential equations of motion [4]

$$[i\partial_z - h(z)]G(z, z') = \delta(z, z') + \int_\gamma d\bar{z} \Sigma(z, \bar{z}) G(\bar{z}, z') \quad (2.6)$$

$$G(z, z') \left[-i \overleftarrow{\partial}_{z'} - h(z') \right] = \delta(z, z') + \int_\gamma d\bar{z} G(z, \bar{z}) \Sigma(\bar{z}, z') \quad (2.7)$$

where all objects are matrices with respect to the basis of one-particle states $\{\varphi(\mathbf{r})\}$. The self-energy Σ accounts for the electronic interactions. Depending on the arguments z, z' ,

the Green's function, $G(z, z')$, and the self-energy, $\Sigma(z, z')$, defined on the time contour have components lesser ($<$), greater ($>$), retarded (R), advanced (A), left ($\bar{}$), right ($\bar{}$) and Matsubara (M) [4]. Typically, one concentrates on the particle and hole propagation in terms of $G^<(t, t')$ and $G^>(t, t')$ where the time arguments t and t' refer to the (real) times when a particle is added or removed from the system. Furthermore, the one-particle reduced density matrix (1RDM) is $\rho(t) \equiv -iG^<(t, t)$ from which one could compute the expectation value of any one-body operator. Taking the equal-time limit ($t' \rightarrow t^+$) one obtains from Eqs. (2.6) and (2.7)

$$i \frac{d}{dt} G^<(t, t) = [h(t) + \Sigma_{\text{HF}}(t), G^<(t, t)] + I(t), \quad (2.8)$$

where we defined the collision integral

$$I(t) = \int_{t_0}^t d\bar{t} [\Sigma_c^>(t, \bar{t}) G^<(\bar{t}, t) - \Sigma_c^<(t, \bar{t}) G^>(\bar{t}, t) + G^<(t, \bar{t}) \Sigma_c^>(\bar{t}, t) - G^>(t, \bar{t}) \Sigma_c^<(\bar{t}, t)]. \quad (2.9)$$

In addition, in Eq. (2.8) we separated the time-local and time-non-local contributions to the self-energy as $\Sigma = \Sigma_{\text{HF}} + \Sigma_c$, the former being referred to as the Hartree-Fock (HF) self-energy and the latter the correlation self-energy, see Fig. 1. This allows for the extraction of a time-local effective single-particle Hamiltonian, $h(t) + \Sigma_{\text{HF}}(t)$. The collision integrals therefore incorporate only the correlation self-energies Σ_c . Importantly, the self-energies depend on the Green's functions themselves, $\Sigma[G]$, and therefore the equation of motion needs to be solved self-consistently. The correlation self-energies are typically obtained by a diagrammatic expansion where terms can be systematically summed up to infinite order. In this work we concentrate on the second-Born self-energy, $\Sigma_c = \Sigma_{2\text{B}}$, see Fig. 1, but the consideration can be extended to other (higher order) diagrams as well.

Although we reduced the considered information to the description of a single-time object ρ , the double-time nature of the full equations of motion is still present in the collision integral which requires the double-time history of Σ^{\lessgtr} and G^{\lessgtr} to be stored. In order to obtain a closed equation for ρ it is customary to use the GKBA [35]

$$G^{\lessgtr}(t, t') \approx i \left[G^{\text{R}}(t, t') G^{\lessgtr}(t', t') - G^{\lessgtr}(t, t) G^{\text{A}}(t, t') \right], \quad (2.10)$$

and an approximation to the double-time propagators $G^{\text{R/A}}$ at the HF level [5]

$$G^{\text{R/A}}(t, t') \approx \mp i \theta[\pm(t - t')] T e^{-i \int_{t_0}^t d\bar{t} [h(\bar{t}) + \Sigma_{\text{HF}}(\bar{t})]}, \quad (2.11)$$

where T is the chronological time-ordering operator [4]. The HF self-energy, being time-local, can be evaluated from the 1RDM as (see Fig. 1)

$$(\Sigma_{\text{HF}})_{ij}(t) = \sum_{kl} (2v_{iklj} - v_{ikjl}) \rho_{lk}(t). \quad (2.12)$$

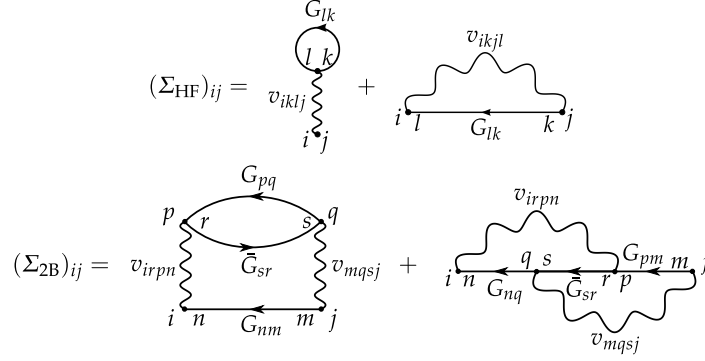


Figure 1: Diagrammatic representations of the Hartree-Fock and the second-Born correlation self-energies. The straight lines denote electronic Green's functions whereas the wiggly lines denote the electronic interactions. The internal indices are summed over. Each diagram comes with a prefactor $(-1)^{N_{\text{loop}}+N_{\text{int}}}$ where N_{loop} is the number of loops and N_{int} is the number of interaction lines [4]. The direct terms with a loop furthermore take an overall spin-degeneracy factor ζ , which in this case is $\zeta = 2$ [49, 50].

The lesser Green's function or the 1RDM can then be solved from Eq. (2.8) by a numerical time-stepping algorithm and using the symmetry property $G^>(t, t) = -i + G^<(t, t)$ [25, 36, 48].

In principle, the collision integral on the vertical branch of the Keldysh contour, $I^{\text{ic}}(t) = -i \int_0^\beta d\tau \Sigma_c^\dagger(t, \tau) G^\dagger(\tau, t)$, should also be taken into consideration. However, using the GKBA, the initial correlations collision integral, I^{ic} , is usually neglected due to the lack of a GKBA-like expression for the mixed components $G^{\dagger, \dagger}$ and $\Sigma_c^{\dagger, \dagger}$. The correlated initial state therefore needs to be prepared by starting with an uncorrelated (or HF) system and slowly switching on the interaction (adiabatic switching procedure) [25, 36, 48, 51]. However, the inclusion of the initial correlations has been shown to be possible also within GKBA [52–54].

3 Second-Born self-energy

For the time-propagation of Eq. (2.8) we are only concerned with the lesser and greater components of the Green's function and self-energy. For the sake of notational simplicity, we then write $G \equiv G^<(t, t')$, $\bar{G} \equiv G^>(t', t)$, and $\Sigma \equiv \Sigma_c^<(t, t')$. In the second-Born approximation (2B) the correlation self-energy takes the form [41, 48] (see Fig. 1)

$$\Sigma_{ij} = 2 \sum_{\substack{mn \\ pq \\ rs}} v_{irpn} v_{mqsj} G_{nm} \bar{G}_{sr} G_{pq} - \sum_{\substack{mn \\ pq \\ rs}} v_{irpn} v_{mqsj} G_{nq} \bar{G}_{sr} G_{pm}. \quad (3.1)$$

As can be seen from Eq. (3.1) computing the full self-energy matrix by direct looping takes N_b^8 operations where N_b is the size of the basis. However, it is possible to reduce this scaling to $\propto N_b^5$ by grouping and reorganizing the objects in Eq. (3.1) [41]. We address this more thoroughly in Sec. 3.3. It is also to be noted that the 2B self-energy is non-local in time, i.e., this computation needs to be performed for two times t and t' , and it is important to keep track of the correct time arguments in the objects v , G and \bar{G} .

Next, we consider three different cases for the interaction vertex: (1) Diagonal basis where the Coulomb integrals take the Hubbard-like form $v_{ijkl} = U_i \delta_{ij} \delta_{ik} \delta_{il}$; (2) Symmetric basis where the Coulomb integrals allow for non-diagonal or long-range interactions $v_{ijkl} = V_{ij} \delta_{il} \delta_{jk}$ but the 4-point vertex is symmetric (density-density type interaction); and (3) The general basis of the full Coulomb integral v_{ijkl} . From the resulting structures of the internal summations in the self-energy diagrams, we identify matrix or tensor operations. Instead of simply looping over the basis indices, employing well-established linear algebra libraries for the matrix and tensor operations [43–45] may speed up the construction of the self-energy.

We denote matrix multiplication by “ \times ” and entrywise multiplication (Hadamard or Schur product) by “ \circ ”. For example, in `Fortran` and `Mathematica` the entrywise products are done through simple multiplication operator “ $*$ ” whereas the matrix product is done through the “`matmul`” or “`.`” operators. In `C++` with the `Armadillo` library [55] the symbol “`%`” is used for entrywise products whereas “ $*$ ” is a matrix product. In `Python` with the `NumPy` (`np`) numerical library [56] the entrywise product can be done with the function “`np.multiply`” whereas the matrix or more general tensor multiplication can be done via the “`np.dot`” or the “`np.einsum`” functions.

3.1 Diagonal basis

For a diagonal basis, $v_{ijkl} = U_i \delta_{ij} \delta_{ik} \delta_{il}$, Eq. (3.1) is simplified as

$$\Sigma_{ij} = U_i U_j G_{ij} \bar{G}_{ji} G_{ij}, \quad (3.2)$$

and the computational cost of constructing the full matrix therefore scales as N_b^2 . In this simple case there are no further contractions to perform as the internal summations were already explicitly resolved due to the Kronecker δ 's in the interaction vertex. Because in many practical implementations entrywise multiplication between two objects is only possible when they have the same dimension, we rewrite the on-site interaction U_i instead as the diagonal part V_{ii} of a matrix. The resulting expression can then be recasted in matrix form as an entrywise product

$$\Sigma = \text{diag}(V) \circ \text{diag}(V) \circ G \circ \bar{G}^T \circ G. \quad (3.3)$$

We anticipate that this is a faster construction for the whole self-energy matrix instead of looping over the basis indices i, j in Eq. (3.2) when passing the matrix operations in Eq. (3.3) to an external linear algebra library.

3.2 Symmetric basis

For a symmetric basis, $v_{ijkl} = V_{ij}\delta_{il}\delta_{jk}$, Eq. (3.1) is simplified as

$$\Sigma_{ij} = 2\sum_{kl} V_{ik}V_{jl}G_{ij}\bar{G}_{lk}G_{kl} - \sum_{kl} V_{ik}V_{jl}G_{il}\bar{G}_{lk}G_{kj}. \quad (3.4)$$

We first consider the first term of Eq. (3.4), i.e., the second-order bubble diagram, and visualize the contraction path for efficient computation. The expression can be manipulated as

$$\begin{aligned} \Sigma_{ij}^b &= 2\sum_{kl} V_{ik}V_{jl}G_{ij}(\bar{G}^T)_{kl}G_{kl} = 2\sum_{kl} V_{ik}V_{jl}G_{ij}(\bar{G}^T \circ G)_{kl} \\ &= 2\sum_l V_{jl}G_{ij} \sum_k V_{ik}(\bar{G}^T \circ G)_{kl} = 2\sum_l V_{jl}G_{ij}[V \times (\bar{G}^T \circ G)]_{il} \\ &= 2\sum_l V_{jl}G_{ij}\{[V \times (\bar{G}^T \circ G)]^T\}_{li} = 2G_{ij} \sum_l V_{jl}\{[V \times (\bar{G}^T \circ G)]^T\}_{li} \\ &= 2G_{ij}(V \times \{[V \times (\bar{G}^T \circ G)]^T\})_{ji} = 2G_{ij}[(V \times \{[V \times (\bar{G}^T \circ G)]^T\})^T]_{ij} \\ &= 2\{G \circ [(V \times \{[V \times (\bar{G}^T \circ G)]^T\})^T]\}_{ij}, \end{aligned} \quad (3.5)$$

where we identified matrix transposes, entrywise products and matrix multiplications. The procedure outlined above, unfortunately, makes the final expressions less readable, but in the end the full self-energy matrix (for the bubble diagram part) may be constructed as a one-liner $\Sigma^b = 2G \circ [(V \times \{[V \times (\bar{G}^T \circ G)]^T\})^T]$. However, as mentioned earlier, one must keep track of the time arguments, i.e., reading from left the first V is evaluated at t' and the second V is evaluated at t .

Contractions on the internal summations in the self-energy diagrams do not always yield a favourable path. If we take the second term in Eq. (3.4), i.e., the second-order exchange diagram, obtaining an expression similar to Eq. (3.5) is not possible for the full self-energy matrix. However, for the diagonal part of the exchange diagram we obtain

$$\begin{aligned} \Sigma_{ii}^x &= -\sum_{kl} V_{ik}V_{il}G_{il}\bar{G}_{lk}G_{ki} = -\sum_l (V \circ G)_{il} \sum_k \bar{G}_{lk}(V^T \circ G)_{ki} \\ &= -\sum_l (V \circ G)_{il} [\bar{G} \times (V^T \circ G)]_{li} = -\{(V \circ G) \times [\bar{G} \times (V^T \circ G)]\}_{ii}. \end{aligned} \quad (3.6)$$

The off-diagonal parts would still need to be evaluated by explicit looping as in Eq. (3.4), but the above contraction path may also be combined with, e.g., the dissection algorithm of Ref. [41] where chosen pairs of the Coulomb integral matrix elements (according to some cut-off energy) would be used. This further reduces the requirement for looping over the basis indices.

3.3 General basis

For a general basis all v_{ijkl} are nonvanishing. In this case the multi-index summations in the self-energy diagrams and their consequent contractions are not always easy to

see, but this task can be automatized using, e.g., the `np.einsum_path` function in Python. The information obtained for an optimal sequence of contractions may further be combined with the symmetry properties (2.4) and with a pre-determined subset of nonzero Coulomb integrals [41].

Manipulating Eq. (3.1) gives

$$\begin{aligned}
\Sigma_{ij} &= 2 \sum_{\substack{np \\ qs}} G_{pq} \underbrace{\sum_m v_{mqsj} G_{nm}}_{\equiv T_{nqsj}^{(1)}} \underbrace{\sum_r v_{irpn} \bar{G}_{sr}}_{\equiv T_{ispn}^{(2)}} - \sum_{\substack{mn \\ ps}} G_{pm} \underbrace{\sum_q \overbrace{v_{mqsj}}^{=v_{qmjs}} G_{nq}}_{=T_{nmjs}^{(1)}} \underbrace{\sum_r v_{irpn} \bar{G}_{sr}}_{=T_{ispn}^{(2)}} \\
&= 2 \sum_{nqs} T_{nqsj}^{(1)} \underbrace{\sum_p G_{pq} T_{ispn}^{(2)}}_{\equiv T_{isqn}^{(3)}} - \sum_{mns} T_{nmjs}^{(1)} \underbrace{\sum_p G_{pm} T_{ispn}^{(2)}}_{\equiv T_{ismn}^{(3)}} \\
&= \sum_{nqs} (2T_{nqsj}^{(1)} T_{isqn}^{(3)} - T_{qnjs}^{(1)} T_{isnq}^{(3)}), \tag{3.7}
\end{aligned}$$

where we defined tensor contractions $T^{(1,2,3)}$ and permuted indices with the help of Eq. (2.4), identifying similar contractions consequently. We see from the last line of Eq. (3.7) that for constructing the full self-energy matrix the scaling over the basis is reduced from N_b^8 to $\propto N_b^5$ [41].

As before, the readability of the self-energy in Eq. 3.7 suffers a bit compared to Fig. 1 or Eq. (3.1). However, Eq. (3.7) is visualized in Fig. 2, and for the sake of efficient computation the contraction operations can be grouped together and executed essentially as a single command, where the lower-level loop fusions and orderings of operations are handled by the underlying numerical library. We note in passing that other contraction paths than the one shown in Fig. 2 are also possible.

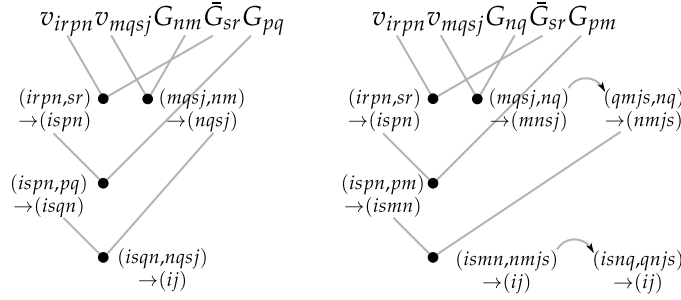


Figure 2: Contraction paths for the computation of the self-energy in Eq. (3.7). The dots denote tensor-contraction operations which could be implemented, e.g., using the `np.einsum` function in Python which includes (from version 1.14 onwards) optimized ordering and dispatching many operations to canonical BLAS routines [57].

4 Numerical benchmarks

For the three different cases presented in the previous section, (1) diagonal, (2) symmetric and (3) general bases, we now present sample numerical simulations for the purpose of benchmarking and assessing the validity and accuracy of the alternative implementations of the 2B self-energy. For test cases we choose molecular systems falling into each of the categories: 1D Hubbard chains which can be related to, e.g., conjugated polymers [51, 58–60] with local (1) and long-range interactions (2). We set the hopping energy between nearest-neighbors $J = -1$, the on-site electron-electron interaction $U = 1$, and the long-range interaction between particles at atomic sites i and j as in the Ohno model $V_{ij} = U/\sqrt{1+|i-j|^2}$ [61, 62]. For the case (3) we take a CH₄ molecule with a general one-particle Kohn-Sham basis obtained from Octopus [63].

We implement the explicit loops over the basis indices [Eqs. (3.2), (3.4), and (3.7)] in C++. In the cases (1) and (2) we employ the matrix operations [Eqs. (3.3), (3.5), and (3.6)] using the Armadillo library (version 9.200.5) [55], and in the case (3) we employ the tensor operations [Eq. (3.7) and Fig. 2] using the NumPy library (version 1.15.1) in Python [56]. We perform the comparisons using a regular desktop computer with an Intel Core i5-4460 @ 3.2 GHz with 6 MB cache, running on 64-bit architecture using Ubuntu 18.04 operating system incorporating the Linux kernel 4.15.0 and the GCC 7.3.0 compiler. The comparisons are done using only a single core to better benchmark the computational cost.

We perform a time-propagation à la GKBA of N_t time steps with length δ . For the sake of simpler computation, in this work we do not employ any predictor-corrector schemes. For the polymer chain we take $N_b = 10$ atomic sites and start the time-propagation from an initial state where $N_b/2$ particles are trapped to the $N_b/2$ leftmost sites by applying a strong confinement potential [51]. This configuration relaxes once the time evolution is started. For the CH₄ molecule we represent the 4 electrons by $N_b = 10$ basis functions, and we start the time-propagation from a HF initial state, which can be obtained from a separate (time-independent) calculation, and then suddenly switch on the many-body correlations in the 2B self-energy. This sudden process can be interpreted as an interaction quench introducing transient dynamics.

For the case (1) we take $N_t = 5000$ time steps of length $\delta = 0.01$, for the case (2) $N_t = 2000$ time steps of length $\delta = 0.025$, and for the case (3) we take $N_t = 1000$ time steps of length $\delta = 0.05$. The reason for the varying number of time steps between the investigated cases is that a calculation with $N_t = 1000$ would be too fast to execute in case (1) for a meaningful comparison of runtimes, whereas $N_t > 1000$ in case (3) would lead to unpractically long execution times for the sake of the present study. Here we are not too concerned about the physical mechanisms taking place during the transient oscillations or how accurate the 2B self-energy is compared to more sophisticated approximations, but our aim is simply to assess the validity of the proposed computation scheme, and to compare execution runtimes.

In Fig. 3 we show the transient dynamics of the three cases discussed above. The execution runtimes for each of these simulations are shown in Tab. 1. We confirm that

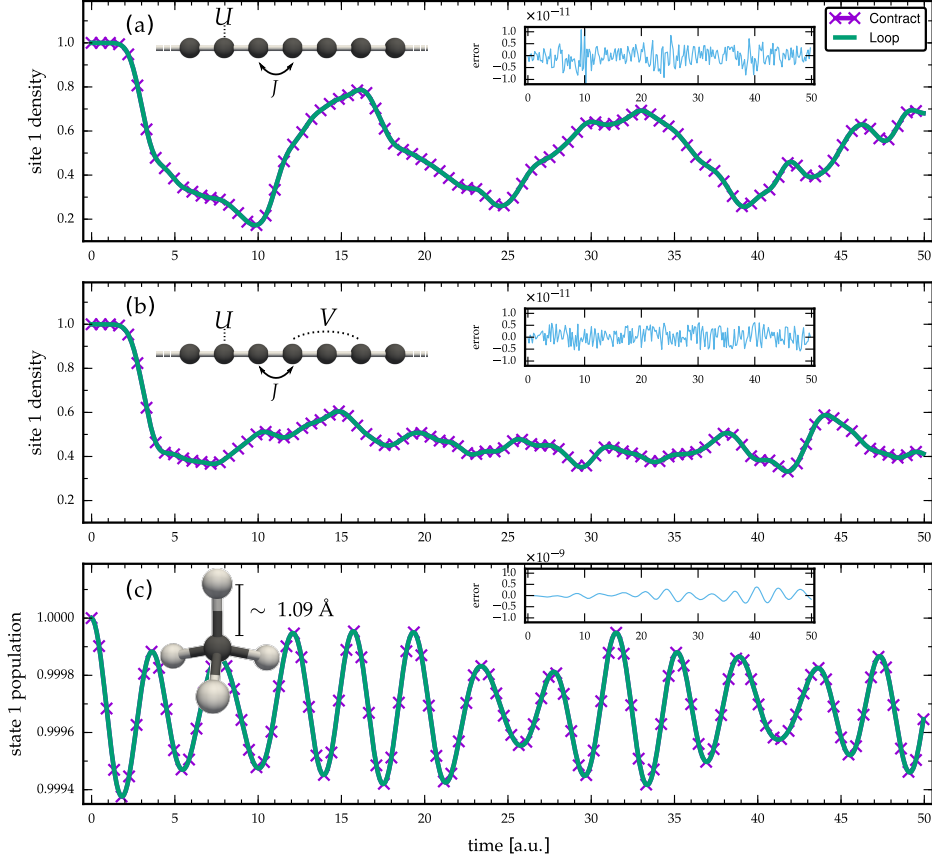


Figure 3: Time-dependent 1RDM elements for the three different systems studied: (a) Diagonal basis with local interaction, (b) Symmetric basis with local and long-range interaction, and (c) General basis with the full Coulomb integrals. The insets show the relative difference between the two curves in the main plots.

within numerical accuracy, both looping over the basis indices and employing tensor-contraction operations, give the same result. Importantly, the execution runtimes are brought down by employing the tensor-contraction operations in the computation of the 2B self-energy. Furthermore, we have checked by increasing the number of time steps that the runtimes increase accordingly, i.e., the gain factors in Tab. 1 remain roughly similar. For additional validation we have compared our data in Fig. 3(c) against the CHEERS code [42] and we find perfect agreement. We note in passing that an ill-advised looping over the full basis in Eq. (3.1) ($\propto N_b^8$) instead of the reduced looping in Eq. (3.7) ($\propto N_b^5$) would result in considerably higher execution runtimes.

As the number of basis functions $N_b = 10$ was relatively small in the previous calculations, we expect increase in the gain factors when larger basis is used, due to profiting

Basis	Scaling	Time (loop)	Time (contr.)	Gain
diagonal	N_b^2	177	164	1.08
symmetric	N_b^4	1213	731	1.66
general	N_b^5	1527	1333	1.15

Table 1: Comparison of serial runtimes (in seconds) of sample simulations of basis size $N_b = 10$ when calculating the self-energy by looping over the basis indices or employing tensor-contraction operations. The gain factor is defined as the ratio of the runtimes. (Note that different number of time steps is taken for the different lines for better comparison of the runtimes.)

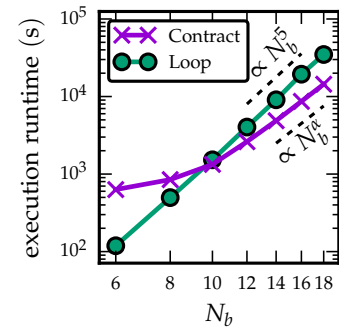


Figure 4: Runtime scaling.

more from the optimized underlying numerical libraries. In Fig. 4 we show the execution runtimes corresponding to Fig. 3(c) but with varying number of basis functions. With explicit looping over the basis indices we observe $\propto N_b^5$ behaviour. For smaller basis sizes the explicit looping is faster compared to the tensor-contraction operations done on the NumPy arrays. However, for larger basis sizes the runtimes using the tensor-contraction operations are significantly smaller, also following a power law behaviour $\propto N_b^\alpha$ for which we empirically find $\alpha \approx 4.3$, see Fig. 4. This reduced scaling could be related to the optimization of matrix multiplication using Strassen [64] or Coppersmith–Winograd [65] algorithms, and to more advanced methods for tensor contraction algorithms which can scale faster than the naïve looping scheme [45].

5 Conclusion

We presented an efficient way to compute the 2B self-energy diagrams, in the NEGF approach, by using tensor-contraction operations. The apparent attraction for efficient computation of the 2B self-energy, in particular, was due to the maximal speed-up in computational scaling when used together with the GKBA. The internal summations in the self-energy calculations were transformed into matrix and tensor operations to be performed by external low-level linear algebra libraries, speeding up the computation. We anticipate the speedup may be even more advantageous when the code is executed in parallel, taking full advantage of the optimized underlying numerical libraries. Instead of looping over the basis indices, utilizing efficiently optimized external numerical libraries for the tensor-contraction operations has the further advantage of speeding up the computation if/when future implementations of the the external libraries become faster and even more efficient [45].

The presented approach is not limited to the 2B self-energy only but could be readily used for other correlation self-energies, such as GW or T -matrix. In addition, many other similar multi-index operations, such as evaluating the initial correlations collision

integral in Ref. [53], might become computationally more accessible by using the tensor-contraction representations. The presented simulations in selected molecular systems provided concrete evidence of the accuracy and applicability of the tensor-contraction operations. With reasonable and precise implementations or variations of the present study, we expect this procedure to allow for considerably larger basis sizes to be possible to address in forthcoming NEGF+first principles simulations.

Acknowledgments

R.T. and M.A.S. acknowledge funding by the DFG (Grant No. SE 2558/2-1) through the Emmy Noether program. We wish to thank Damian Hofmann, Gianluca Stefanucci and Angel Rubio for productive discussions.

References

- [1] G. Baym and L. P. Kadanoff. Conservation Laws and Correlation Functions. *Phys. Rev.*, 124 (1961), 287–299.
- [2] L. P. Kadanoff and G. Baym. *Quantum Statistical Mechanics*. W. A. Benjamin, New York, 1962.
- [3] P. Danielewicz. Quantum theory of nonequilibrium processes, I. *Ann. Phys. (N. Y.)*, 152 (1984), 239–304.
- [4] G. Stefanucci and R. van Leeuwen. *Nonequilibrium Many-Body Theory of Quantum systems: A Modern Introduction*. Cambridge University Press, Cambridge, 2013.
- [5] K. Balzer and M. Bonitz. *Nonequilibrium Green’s Functions Approach to Inhomogeneous Systems*. Springer Berlin Heidelberg, 2013.
- [6] H. S. Köhler, N. H. Kwong and H. A. Yousif. A Fortran code for solving the Kadanoff–Baym equations for a homogeneous fermion system. *Comp. Phys. Commun.*, 123 (1999), 123–142.
- [7] D. Semkat, D. Kremp and M. Bonitz. Kadanoff-Baym equations with initial correlations. *Phys. Rev. E*, 59 (1999), 1557–1562.
- [8] N.-H. Kwong and M. Bonitz. Real-Time Kadanoff-Baym Approach to Plasma Oscillations in a Correlated Electron Gas. *Phys. Rev. Lett.*, 84 (2000), 1768–1771.
- [9] W. H. Dickhoff and C. Barbieri. Self-consistent Green’s function method for nuclei and nuclear matter. *Prog. Part. Nucl. Phys.*, 52 (2004), 377–496.
- [10] A. Rios, B. Barker, M. Buchler and P. Danielewicz. Towards a nonequilibrium Green’s function description of nuclear reactions: One-dimensional mean-field dynamics. *Ann. Phys. (N. Y.)*, 326 (2011), 1274–1319.
- [11] N. E. Dahlen and R. van Leeuwen. Solving the Kadanoff-Baym Equations for Inhomogeneous Systems: Application to Atoms and Molecules. *Phys. Rev. Lett.*, 98 (2007), 153004.
- [12] M. Galperin, M. A. Ratner and A. Nitzan. Molecular transport junctions: vibrational effects. *J. Phys. Condens. Matter*, 19 (2007), 103201.
- [13] E. Perfetto, A.-M. Uimonen, R. van Leeuwen and G. Stefanucci. First-principles nonequilibrium Green’s-function approach to transient photoabsorption: Application to atoms. *Phys. Rev. A*, 92 (2015), 033419.

- [14] F. Covito, E. Perfetto, A. Rubio and G. Stefanucci. Benchmarking nonequilibrium Green's functions against configuration interaction for time-dependent Auger decay processes. *Eur. Phys. J. B*, 91 (2018), 216.
- [15] J. K. Freericks, H. R. Krishnamurthy and T. Pruschke. Theoretical Description of Time-Resolved Photoemission Spectroscopy: Application to Pump-Probe Experiments. *Phys. Rev. Lett.*, 102 (2009), 136401.
- [16] B. Moritz, A. F. Kemper, M. Sentef, T. P. Devereaux and J. K. Freericks. Electron-Mediated Relaxation Following Ultrafast Pumping of Strongly Correlated Materials: Model Evidence of a Correlation-Tuned Crossover between Thermal and Nonthermal States. *Phys. Rev. Lett.*, 111 (2013), 077401.
- [17] A. F. Kemper, M. Sentef, B. Moritz, C. C. Kao, Z. X. Shen, J. K. Freericks and T. P. Devereaux. Mapping of unoccupied states and relevant bosonic modes via the time-dependent momentum distribution. *Phys. Rev. B*, 87 (2013), 235139.
- [18] M. Sentef, A. F. Kemper, B. Moritz, J. K. Freericks, Z.-X. Shen and T. P. Devereaux. Examining electron-boson coupling using time-resolved spectroscopy. *Phys. Rev. X*, 3 (2013), 041033.
- [19] H. Aoki, N. Tsuji, M. Eckstein, M. Kollar, T. Oka and P. Werner. Nonequilibrium dynamical mean-field theory and its applications. *Rev. Mod. Phys.*, 86 (2014), 779–837.
- [20] A. F. Kemper, M. A. Sentef, B. Moritz, J. K. Freericks and T. P. Devereaux. Effect of dynamical spectral weight redistribution on effective interactions in time-resolved spectroscopy. *Phys. Rev. B*, 90 (2014), 075126.
- [21] A. F. Kemper, M. A. Sentef, B. Moritz, J. K. Freericks and T. P. Devereaux. Direct observation of Higgs mode oscillations in the pump-probe photoemission spectra of electron-phonon mediated superconductors. *Phys. Rev. B*, 92 (2015), 224517.
- [22] M. A. Sentef, A. F. Kemper, A. Georges and C. Kollath. Theory of light-enhanced phonon-mediated superconductivity. *Phys. Rev. B*, 93 (2016), 144506.
- [23] D. Golež, P. Werner and M. Eckstein. Photoinduced gap closure in an excitonic insulator. *Phys. Rev. B*, 94 (2016), 035121.
- [24] A. F. Kemper, M. A. Sentef, B. Moritz, T. P. Devereaux and J. K. Freericks. Review of the Theoretical Description of Time-Resolved Angle-Resolved Photoemission Spectroscopy in Electron-Phonon Mediated Superconductors. *Ann. Phys. (Berl.)*, 529 (2017), 1600235.
- [25] R. Tuovinen, D. Golež, M. Schler, P. Werner, M. Eckstein and M. A. Sentef. Adiabatic Preparation of a Correlated Symmetry-Broken Initial State with the Generalized Kadanoff-Baym Ansatz. *Phys. Status Solidi B*, (2018). doi:10.1002/pssb.201800469.
- [26] M. Brandbyge, J.-L. Mozos, P. Ordejón, J. Taylor and K. Stokbro. Density-functional method for nonequilibrium electron transport. *Phys. Rev. B*, 65 (2002), 165401.
- [27] M. F. Ludovico and L. Arrachea. Conductance oscillations in a mesoscopic ring threaded by a harmonically time-dependent magnetic flux. *Phys. B Condens. Matter*, 407 (2012), 3256–3258.
- [28] J.-S. Wang, B. K. Agarwalla, H. Li and J. Thingna. Nonequilibrium Green's function method for quantum thermal transport. *Front. Phys.*, 9 (2014), 673–697.
- [29] M. Ridley and R. Tuovinen. Time-dependent Landauer-Büttiker approach to charge pumping in ac-driven graphene nanoribbons. *Phys. Rev. B*, 96 (2017).
- [30] R. Tuovinen, E. Perfetto, R. van Leeuwen, G. Stefanucci and M. A. Sentef. Distinguishing Majorana Zero Modes from Impurity States through Time-Resolved Transport. arXiv:1902.05821, (2019).
- [31] R. Tuovinen, M. A. Sentef, C. G. da Rocha and M. S. Ferreira. Time-resolved impurity-invisibility in graphene nanoribbons. arXiv:1903.12538, (2019).

- [32] K. Kainulainen, T. Prokopec, M. G. Schmidt and S. Weinstock. Semiclassical force for electroweak baryogenesis: Three-dimensional derivation. *Phys. Rev. D*, 66 (2002), 043502.
- [33] M. Garny and M. M. Müller. Kadanoff-Baym equations with non-Gaussian initial conditions: The equilibrium limit. *Phys. Rev. D*, 80 (2009), 085011.
- [34] M. Garny, A. Kartavtsev and A. Hohenegger. Leptogenesis from first principles in the resonant regime. *Ann. Phys. (N. Y.)*, 328 (2013), 26–63.
- [35] P. Lipavský, V. Špička and B. Velický. Generalized Kadanoff-Baym ansatz for deriving quantum transport equations. *Phys. Rev. B*, 34 (1986), 6933.
- [36] S. Hermanns, K. Balzer and M. Bonitz. The non-equilibrium Green function approach to inhomogeneous quantum many-body systems using the generalized Kadanoff-Baym ansatz. *Phys. Scr.*, 2012 (2012), 014036.
- [37] V. M. Galitskii. The Energy Spectrum of a Non-ideal Fermi Gas. *Sov. Phys. JETP*, 7 (1958), 104.
- [38] L. Hedin. New Method for Calculating the One-Particle Green's Function with Application to the Electron-Gas Problem. *Phys. Rev.*, 139 (1965), A796.
- [39] M. P. von Friesen, C. Verdozzi and C.-O. Almbladh. Successes and Failures of Kadanoff-Baym Dynamics in Hubbard Nanoclusters. *Phys. Rev. Lett.*, 103 (2009), 176404.
- [40] A. A. Rusakov and D. Zgid. Self-consistent second-order Green's function perturbation theory for periodic systems. *J. Chem. Phys.*, 144 (2016), 054106.
- [41] E. Perfetto and G. Stefanucci. The Dissection Algorithm for the Second-Born Self-Energy. *Phys. Status Solidi B*, (2019). doi:10.1002/pssb.201800573.
- [42] E. Perfetto and G. Stefanucci. CHEERS: a tool for correlated hole-electron evolution from real-time simulations. *J. Phys. Condens. Matter*, 30 (2018), 465901.
- [43] G. Baumgartner, A. Auer, D. E. Bernholdt, A. Bibireata, V. Choppella, D. Cociorva, R. J. Harrison, S. Hirata, S. Krishnamoorthy, S. Krishnan, M. Nooijen, R. M. Pitzer, J. Ramanujam, P. Sadayappan and A. Sibiryakov. Synthesis of High-Performance Parallel Programs for a Class of ab Initio Quantum Chemistry Models. *Proc. IEEE*, 93 (2005), 276–292.
- [44] E. Solomonik, D. Matthews, J. R. Hammond, J. F. Stanton and J. Demmel. A massively parallel tensor contraction framework for coupled-cluster computations. *J. Parallel Distrib. Comput.*, 74 (2014), 3176–3190.
- [45] J. Huang, D. Matthews and R. van de Geijn. Strassen's Algorithm for Tensor Contraction. *SIAM J. Sci. Comput.*, 40 (2018), C305–C326.
- [46] P. Myöhänen, A. Stan, G. Stefanucci and R. van Leeuwen. A many-body approach to quantum transport dynamics: Initial correlations and memory effects. *EPL*, 84 (2008), 67001.
- [47] P. Myöhänen, A. Stan, G. Stefanucci and R. van Leeuwen. Kadanoff-Baym approach to quantum transport through interacting nanoscale systems: From the transient to the steady-state regime. *Phys. Rev. B*, 80 (2009), 115107.
- [48] S. Latini, E. Perfetto, A.-M. Uimonen, R. van Leeuwen and G. Stefanucci. Charge dynamics in molecular junctions: Nonequilibrium Green's function approach made fast. *Phys. Rev. B*, 89 (2014), 075306.
- [49] H. Bruus and K. Flensberg. *Many-Body Quantum Theory in Condensed Matter Physics*. Oxford University Press, New York, 2007.
- [50] K. Balzer. Solving the Two-time Kadanoff-Baym Equations. Application to Model Atoms and Molecules. Ph.D. thesis, Christian-Albrechts-Universität zu Kiel, 2011.
- [51] S. Hermanns, N. Schlünzen and M. Bonitz. Hubbard nanoclusters far from equilibrium. *Phys. Rev. B*, 90 (2014), 125111.
- [52] D. Semkat, M. Bonitz and D. Kremp. Relaxation of a quantum many-body system from a

- correlated initial state. A general and consistent approach. *Contrib. Plasma Phys.*, 43 (2003), 321–325.
- [53] D. Karlsson, R. van Leeuwen, E. Perfetto and G. Stefanucci. The generalized Kadanoff-Baym ansatz with initial correlations. *Phys. Rev. B*, 98 (2018), 115148.
- [54] M. Hopjan and C. Verdozzi. Initial correlated states for the generalized Kadanoff-Baym Ansatz without adiabatic switching-on of interactions in closed systems. *Eur. Phys. J. Spec. Top.*, 227 (2019), 1939–1948.
- [55] C. Sanderson and R. Curtin. Armadillo: a template-based C++ library for linear algebra. *J. Open Source Softw.*, 1 (2016), 26.
- [56] T. E. Oliphant. A guide to NumPy. Trelgol Publishing, USA, 2006.
- [57] D. G. A. Smith and J. Gray. `opt_einsum` - A Python package for optimizing contraction order for einsum-like expressions. *J. Open Source Softw.*, 3 (2018), 753.
- [58] B. Kirtman and B. Champagne. Nonlinear optical properties of quasilinear conjugated oligomers, polymers and organic molecules. *Int. Rev. Phys. Chem.*, 16 (1997), 389–420.
- [59] M. van Faassen, P. L. de Boeij, R. van Leeuwen, J. A. Berger and J. G. Snijders. Ultranonlocality in Time-Dependent Current-Density-Functional Theory: Application to Conjugated Polymers. *Phys. Rev. Lett.*, 88 (2002), 186401.
- [60] M. van Faassen, P. L. de Boeij, R. van Leeuwen, J. A. Berger and J. G. Snijders. Application of time-dependent current-density-functional theory to nonlocal exchange-correlation effects in polymers. *J. Chem. Phys.*, 118 (2003), 1044–1053.
- [61] K. Ohno. Some remarks on the Pariser-Parr-Pople method. *Theoret. Chim. Acta*, 2 (1964), 219–227.
- [62] D. Baeriswyl, D. K. Campbell and S. Mazumdar. An Overview of the Theory of π -Conjugated Polymers. In H. G. Giess, editor, *Conjugated Conducting Polymers*. Springer, 1992.
- [63] M. A. Marques, A. Castro, G. F. Bertsch and A. Rubio. `octopus`: a first-principles tool for excited electron-ion dynamics. *Comput. Phys. Commun.*, 151 (2003), 60–78.
- [64] V. Strassen. Gaussian Elimination is not Optimal. *Numer. Math.*, 13 (1969), 354–356.
- [65] D. Coppersmith and S. Winograd. Matrix multiplication via arithmetic progressions. *J. Symb. Comput.*, 9 (1990), 251–280.